Journal of Materials Chemistry A

PAPER

View Article Online
View Journal | View Issue

Cite this: J. Mater. Chem. A, 2014, 2, 5418

Structural tuning of ancillary chelate in tri-carboxyterpyridine Ru(II) sensitizers for dye sensitized solar cells†

Chun-Cheng Chou,‡[a] Pei-Hua Chen,‡[a] Fa-Chun Hu,[a] Yun Chi,*[a] Shu-Te Ho,[a] Ji-Jung Kai,*[b] Shih-Hung Liu[c] and Pi-Tai Chou*[c]

Received 25th November 2013
Accepted 20th January 2014

DOI: 10.1039/c3ta14876a

www.rsc.org/MaterialsA

Three distinct classes of ancillary chelates, namely: 2-(3-trifluoromethylpyrazol-5-yl)-6-(3-trifluoromethylphenyl)-pyridine (**L3**, H_2pzppy), 4-(3-trifluoromethylpyrazol-5-yl)-2-(3-trifluoromethyl)phenylpyrimidine (**L5**, H_2pzppm) and 4-(6-(3-trifluoromethylpyrazol-5-yl)pyridin-2-yl)-2-trifluoromethylpyrimidine (**L6**, H_2pzpypm), which showed an identical skeletal topology, but with the more electronegative nitrogen atom replacing the isoelectronic methine group at the selected skeletal position, were obtained to investigate the photophysical and electrochemical properties and hence the associated Ru(II) sensitizers based DSCs. To increase the optical absorptivity we also strategically added thiophene (thienyl) or 3,4-ethylenedioxythiophene (EDOT) appendages to **L6**, for boosting the short-circuit photocurrent (J_{SC}) and the overall efficiency (η) of the fabricated DSC devices. Under AM 1.5G illumination, the best sensitizer showed performance data of J_{SC} = 18.11 mA cm^{-2}, V_{OC} = 0.66 V, FF = 0.729 and η = 8.72%, and a good cell stability at 60 °C for 1000 hours, being only decreased by ~5% in the η value.

Introduction

The future prospect of a low-carbon society requires emerging renewable energy sources, among which dye-sensitized solar cells (DSCs) are considered to be one competitive candidate. Especially, the low cost TiO_2 photoanode in DSCs can potentially be fabricated using printing technology, providing a viable alternative to conventional photovoltaics. Despite the development of a vast variety of different dyes to optimize the harvested solar photons, up to the current stage, the Ru(II) based photosensitizers remain the key component, because of the higher cell performance, particularly in view of their stabilities *versus* other sensitizers, such as organic donor-acceptor dyes and zinc porphyrin/phthalocyanine dyes.[1–5] Broadly speaking, the Ru(II) sensitizers constitute at least one di- or tri-carboxy substituted poly-pyridine chelate, to serve as the anchor to the TiO_2 photoanode, plus an ancillary ligand which would modify both the light absorption capacity, ground state oxidation potential, and relative peak position of the metal-to-ligand charge transfer (MLCT) transition. Among a variety of Ru(II) based photosensitizers, the thiocyanate-containing sensitizers N749 (or black dye),[6–8] Z907[9] and N719[10] represent three of the best known examples that have been tested for both fundamental and commercial applications.

From the viewpoint of device stability, the robust skeletal framework of sensitizers is considered as a major factor governing the lifespan. Thus, studies on thiocyanate-free Ru(II) sensitizers with either a dicarboxy bipyridine, or tricarboxy terpyridine anchor, have emerged in recent years.[11–22] The thiocyanate is expected to undergo dissociation from the sensitizer in solution, due to its latent activity against ligand exchange.[23] To mitigate this problem, a new class of Ru(II) sensitizers was synthesized, with the thiocyanate replaced by either an electron-deficient cyclometalate[24–27] or a chelating azolate.[28–30] This approach was stimulated by the general belief that the chelate should be less labile compared to the unidentate bonding of thiocyanate, and the fact that the added electron deficiency is able to increase the ground state oxidation potential of the sensitizers for faster dye regeneration, by I^-/I_3^- redox couple.

Recently, our interests have extended to bis-tridentate Ru(II) sensitizers.[31–35] We started with a series of multidentate ancillary chelates, namely: 2,6-bis(3-trifluoromethylpyrazol-5-yl)pyridine (**L1**, H_2pz_2py), 2,6-bis(3-trifluoromethyl-1,2,4-triazol-5-yl)pyridine (**L2**, H_2tz_2py), 2-(3-trifluoromethylpyrazol-5-yl)-6-(3-trifluoromethylphenyl)pyridine (**L3**, H_2pzppy) and 2-(3-trifluoromethyl-1,2,4-triazol-5-yl)-6-(3-trifluoromethylphenyl)pyridine (**L4**, H_2tzppy), which are synthesized and employed in the construction of

[a]Department of Chemistry and Low Carbon Energy Research Center, National Tsing Hua University, Hsinchu 30013, Taiwan. E-mail: ychi@mx.nthu.edu.tw

[b]Department of Engineering and System Science, National Tsing Hua University, Taiwan. E-mail: jjkai@ess.nthu.edu.tw

[c]Department of Chemistry and Center for Emerging Material and Advanced Devices, National Taiwan University, Taipei 10617, Taiwan. E-mail: chop@ntu.edu.tw

† Electronic supplementary information (ESI) available. See DOI: 10.1039/c3ta14876a

‡ C.-C C. and P.-H C. contributed equally to this work.

relevant Ru(II) sensitizers (see Scheme 1). Their outstanding DSC performances were subsequently validated by showing an optimal light harvesting capability, down to the near-IR region. Motivated by this finding, we then launched a study on synthesizing new multidentate ancillaries to further fine-tune their electrochemical and spectroscopic properties, by the insertion of a nitrogen atom at specific positions on the backbone, and to explore the associated cell performances.

In this paper, we present two new classes of ancillary chelates, namely: 4-(3-trifluoromethylpyrazol-5-yl)-2-(3-trifluoromethyl)phenylpyrimidine (**L5**, H_2pzppm) and 4-(6-(3-trifluoromethylpyrazol-5-yl)pyridin-2-yl)-2-trifluoromethylpyrimidine (**L6**, H_2pzpypm). Their structures differ by the incorporation of one pyrimidine fragment, as opposed to the central pyridine fragment, or at the terminal phenyl group in the parent **L3** ancillary (Scheme 1). We then probe this subtle structural change *versus* the critical effect on the DSC performance. Moreover, substituted thiophene (thienyl) or 3,4-ethylenedioxythiophene (EDOT) appendages were also added to the **L6** ancillary in an aim to increase the optical absorptivity and hence boost the short-circuit photocurrent (J_{SC}) and overall efficiency (η) under AM 1.5G illumination.

Results and discussion

Firstly, the required dianionic tridentate ancillaries were prepared *via* the multi-step protocols depicted in Schemes 2 and 3. For the H_2pzppm chelate **L5**, the first step was to replace the 4-chloro substituent of 2,4-dichloropyrimidine with a methoxide protecting group, by a simple nucleophilic substitution,[36] followed by the replacement of the unprotected 2-chloro substituent with the *m*-trifluoromethylphenyl group, using a Suzuki cross-coupling reaction.[37] The subsequent conversion of the 4-methoxy group back to the chloro substituent was achieved using the chlorination reagent $POCl_3$.[38] The resulting chloride compound was subjected to cyanation using KCN,[39] followed by methylation with a Grignard reagent, to afford the acetyl group.[40] Finally, this acetyl group was converted to the pyrazole moiety using a Claisen condensation and hydrazine cyclization, in sequence.[41]

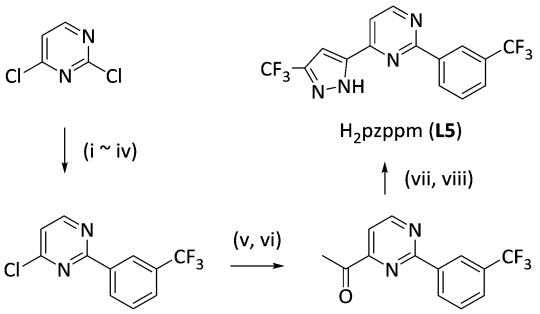

Scheme 2 Synthetic protocols: (i) NaOMe, MeOH; (ii) 3-(trifluoromethyl)phenyl boronic acid, $[Pd(PPh_3)_4]$, Na_2CO_3, THF–H_2O; (iii) $HCl_{(aq)}$; (iv) $POCl_3$, toluene; (v) KCN, DABCO, DMSO–H_2O; (vi) CH_3MgBr, THF, $HCl_{(aq)}$; (vii) NaOEt, CF_3CO_2Et, THF; (viii) N_2H_4, EtOH.

On the other hand, the H_2pzpypm chelate **L6** and its thienyl and EDOT functionalized derivatives, *i.e.* **L6.1**: R = 5-hexyl-2-thienyl and **L6.2**: R = 7-hexyl-2,3-dihydrothieno[3,4-*b*]-1,4-dioxin-5-yl, were prepared using another synthetic sequence, starting from 2,6-diacetylpyridine and its derivatives, see Scheme 3. One acetyl substituent was firstly protected using a stoichiometric amount of ethylene glycol in the presence of an acid catalyst;[42] the second (unprotected) acetyl group was sequentially reacted with *N*,*N*-dimethylformamide dimethyl acetal, trifluoroacetamidine and sodium ethoxide, to induce the formation of a CF_3-substituted pyrimidine fragment.[43] After that, the dioxolane group was hydrolyzed to release the acetyl group.[44] It was then reacted with ethyl trifluoroacetate under conditions for a Claisen condensation, followed by hydrazine cyclization, to afford the anticipated pyrazole group.[41]

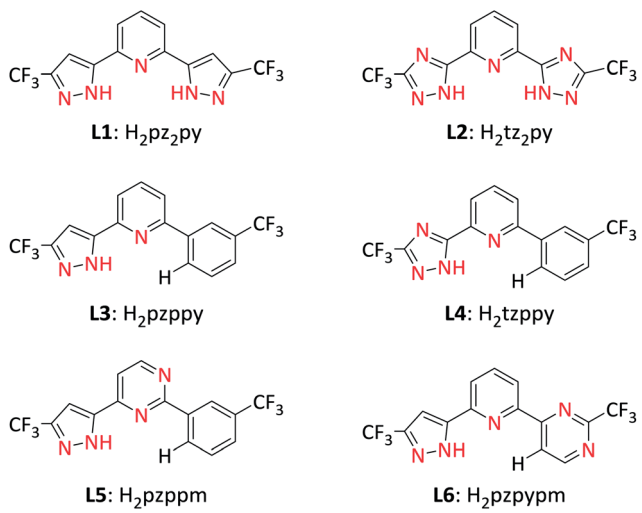

Scheme 1 Structures of the ancillary chelates in various bis-tridentate Ru(II) sensitizers.

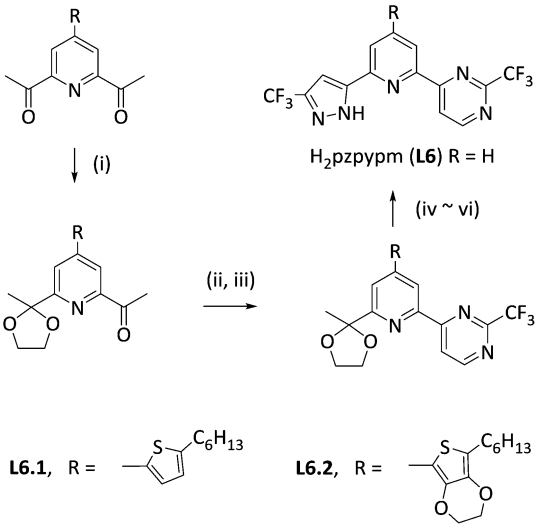

Scheme 3 Synthetic protocols: (i) ethylene glycol; (ii) *N*,*N*-dimethylformamide dimethyl acetal; (iii) trifluoroacetamidine, NaOEt, EtOH; (iv) $HCl_{(aq)}$; (v) NaOEt, CF_3CO_2Et, THF; (vi) N_2H_4, EtOH.

With these ancillary chelates in hand, the required bis-tridentate Ru(II) sensitizers could be synthesized from the coupling of Ru(tectpy)Cl_3 (tectpy = 4,4′,4″-triethoxycarboxy-2,2′:6′,2″-terpyridine) and the ancillary chelate in the presence of KOAc. Specifically, the designated Ru(II) sensitizers **TF-25**, **26**, **27** and **28** were synthesized using the aforementioned chelates **L5**, **L6**, **L6.1** and **L6.2**, respectively. Their molecular structures, together with that of the reference sensitizer **TF-21**, are depicted in Scheme 4.

The UV-vis absorption spectra of the sensitizers **TF-25**–**TF-28** in DMF (*N*,*N*-dimethylformamide) at a concentration of 1×10^{-5} M are depicted in Fig. 1, together with the spectrum of **TF-21** as a reference, while the photophysical and cyclic voltammetric data are listed in Table 1. Generally speaking, **TF-21** exhibited two sharp MLCT bands at 404 nm and 521 nm, together with a longer wavelength shoulder that showed a slow decrease in the intensity and extended to the near infrared (>800 nm). In accordance with this pattern, both **TF-25** and **TF-26** depicted two MLCT absorptions at ~400 and ~520 nm, with the extinction coefficient of the lower energy MLCT band (1.2×10^4 L mol^{-1} cm^{-1}) being slightly lower than that of the higher energy one (1.5×10^4 L mol^{-1} cm^{-1}), with a much faster decline in the intensity for the lower energy MLCT shoulder *versus* that of **TF-21**. Furthermore, upon the addition of the thienyl and EDOT groups to **TF-26**, the resulting sensitizers **TF-27** and **TF-28** gave the lower energy MLCT peak maxima at around 530 and 533 nm, *i.e.* with a bathochromic shift of at least 13 nm *versus* that of **TF-26**, and a substantial gain in the absorptivity to $\varepsilon = 2.1$–2.3×10^4 L mol^{-1} cm^{-1}. This could imply a better light harvesting capability for **TF-27** and **TF-28** over that of the parent **TF-26**, which is consistent with the influence of the attached electron donating and π-conjugating appendage observed in many organic push–pull and Ru(II) based sensitizers.[45–52]

Calculations based on density functional theory (DFT) and time-dependent DFT in DMF were performed for the title complexes. Fig. 2 and 3 depict the simulation of the absorption wavelengths (vertical line) and the relative transition probability (magnitude of the vertical line) of **TF-25**–**TF-28** (see the results of

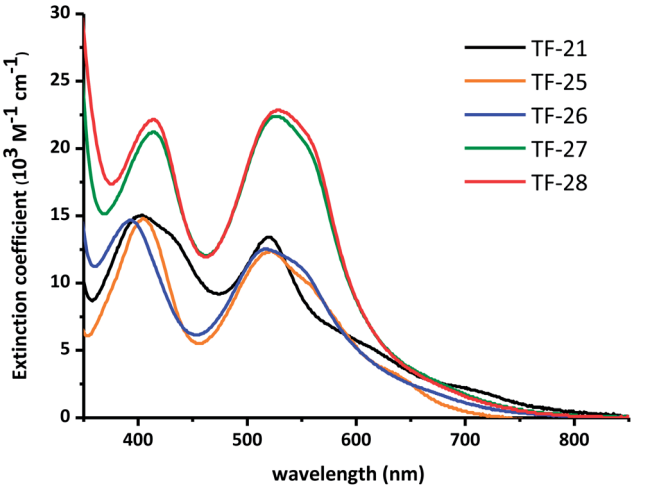

Fig. 1 UV-vis absorption spectra of Ru(II) sensitizers **TF-25**–**TF-28** and reference **TF-21** at 1×10^{-5} M in DMF at RT.

TF-21 in ref. 33). Also depicted in these figures are the frontier orbitals contributing to the major electronic transition recorded. All the numerical data for the vertical transition and comprehensive frontier orbital analyses are listed in Tables S1–S4 and Fig. S1–S4 of the ESI.† As a result, the peak wavelength over 500 nm was calculated to be 529, 521, 522, and 525 nm for **TF-25**–**TF-28**, respectively, for which both the value and trend are consistent with the experimental absorption maximum for **TF-25** (523 nm), **TF-26** (517 nm), **TF-27** (530 nm) and **TF-28** (533 nm) in DMF (see Table 1), supporting the validity of the computational approaches. A careful examination of the optical transition and its associated frontier orbitals indicates that the lower lying singlet transitions over 500 nm are mainly contributed by a metal-to-ligand (tricarboxy-terpyridine) charge transfer (MLCT), together with a minor part of an ancillary to anchor (terpyridine) charge transfer (LLCT). In the higher lying transition, around 400–550 nm, the unoccupied orbitals of the thienyl (**TF-27**) and EDOT (**TF-28**) appendages have imposed an appreciable contribution (see Fig. 3) due to an elongation of the π-conjugation,[53–56] which rationalizes the substantial gain of the absorptivity as well as the red shift of the peak wavelength observed experimentally for **TF-27** and **TF-28** in this region.

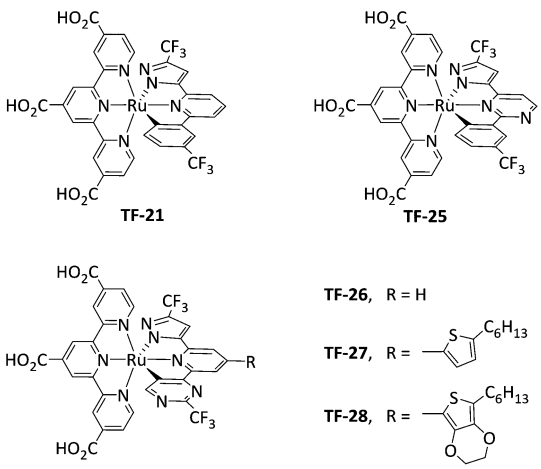

Scheme 4 Structures of Ru(II) sensitizers **TF-25**–**TF-28** and **TF-21** reference.

Table 1 Photophysical and electrochemical data for the studied Ru(II) sensitizers

Dye	λ_{abs}[a] [nm] (ε [10^3 L mol^{-1} cm^{-1}])	$E_{ox}^{\circ\prime}$[b] (V)	E_{0-0} (eV)	$E^{\circ\prime}$* (V)
TF-21	404 (15), 520 (13), 703 (2.2)	0.84	1.62	−0.78
TF-25	405 (15), 523 (12), 555 (10)	0.93	1.72	−0.79
TF-26	393 (15), 517 (12), 548 (11)	0.96	1.75	−0.79
TF-27	415 (21), 530 (22), 558 (20)	0.96	1.72	−0.76
TF-28	415 (22), 533 (23), 558 (21)	0.94	1.74	−0.80

[a] Absorption and emission spectra were measured at 1×10^{-5} M in DMF. [b] Oxidation potential of dyes was measured in DMF with 0.1 M [TBA][PF_6] and a scan rate of 50 mV s^{-1}. It was calibrated with Fc/Fc$^+$ as internal standard and converted to normal hydrogen electrode (NHE) by addition of 0.63 V.

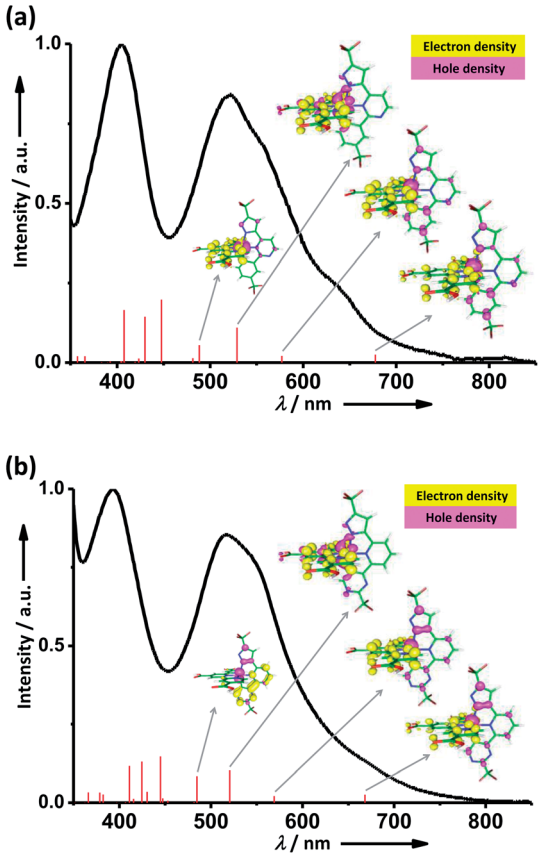

Fig. 2 The absorption spectra of (a) **TF-25** and (b) **TF-26** sensitizers. Also depicted are the TD-DFT calculated absorption wavelengths (vertical line) and the relative transition probability (magnitude of vertical line). Inset: the selected frontier orbitals contributed to the major transitions. The occupied and unoccupied orbitals are represented in pink and yellow, respectively.

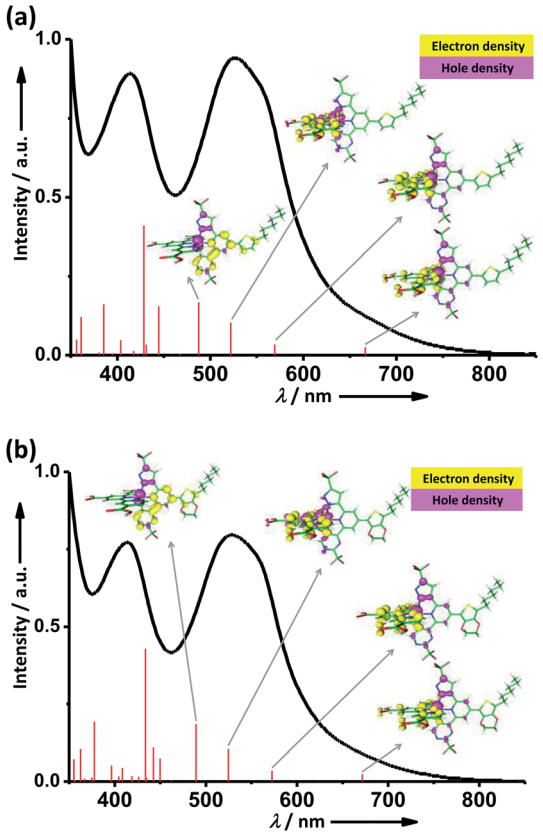

Fig. 3 The absorption spectra of (a) **TF-27** and (b) **TF-28** sensitizers. Also depicted are the TD-DFT calculated absorption wavelengths (vertical line) and the relative transition probability (magnitude of vertical line). Inset: the selected frontier orbitals contributed to the major transitions. The occupied and unoccupied orbitals are represented in pink and yellow, respectively.

Cyclic voltammetry was conducted to reveal the ground state oxidation potential ($E^{\circ\prime}_{ox}$). With the $E^{\circ\prime}_{ox}$ data in hand, the corresponding excited state oxidation potentials ($E^{\circ\prime}$*) were estimated using the equation $E^{\circ\prime}* = E^{\circ\prime}_{ox} - E_{0-0}$, for which E_{0-0} stands for the optical energy gap, *i.e.* at a 5% onset of their lowest energy absorption. In general, the absorption onset of **TF-25** and **TF-26** show a significant hypsochromic shift compared to **TF-21**, resulting in the higher onset energy, by 0.1 eV. However, this increase in E_{0-0} was offset by the more positive $E^{\circ\prime}_{ox}$ of **TF-25** and **TF-26** recorded (0.93 and 0.96 V), leaving the respective $E^{\circ\prime}$* essentially unchanged. Moreover, the **TF-27** and **TF-28** sensitizers were modified by the addition of the thienyl and EDOT appendages to **TF-26**. Although this functionalization red shifts the higher lying MLCT/$\pi\pi$* absorptions, as well as simultaneously increasing the extinction coefficient, their $E^{\circ\prime}_{ox}$ values are virtually unaltered *versus* that of **TF-26** (see Table 1). Moreover, as shown in Fig. 1, the onset of the absorption, *i.e.*, E_{0-0}, is nearly the same among **TF-26**, **TF-27** and **TF-28**. Support of this concept was also provided by the computational results, in which the calculated $S_0 \rightarrow S_1$ transitions are virtually identical, being 668, 666 and 671 nm for **TF-26**, **TF-27** and **TF-28**, respectively (see Tables S2–S4†). The result also reconfirms the aforementioned viewpoint that the added thienyl (**TF-27**) and EDOT (**TF-28**) appendages only affect the higher lying excited state, while the lowest lying excited state is dominated by the Ru(II)-to-anchor (tricarboxy-terpyridine) MLCT transition. The invariance of $E^{\circ\prime}_{ox}$ and E_{0-0} leads to a similar $E^{\circ\prime}$* for **TF-26–28**. For all these newly developed Ru(II) complexes, evidently, the obtained $E^{\circ\prime}_{ox}$ and $E^{\circ\prime}$* are sufficiently more positive and negative than that of the redox potential of an I^-/I_3^- couple (*ca.* 0.35 V *vs.* NHE) as well as the corresponding conduction band edge of the TiO_2 electrode (*ca.* −0.7 V *vs.* NHE)[27,57] respectively, confirming their suitability to serve as suitable DSC sensitizers.

DSCs were next fabricated using these sensitizers absorbed on a TiO_2 photoanode, that consisted of a 15 μm layer of 20 nm absorbing particles and a 7 μm layer of 400 nm light scattering particles, deposited with multiple screen-printing manipulation.[33] Moreover, the sensitizers were dissolved in a mixture of EtOH and DMSO (v/v 4 : 1) to afford a 0.3 mM solution, together with the addition of 1 mM chenodeoxycholic acid (CDCA) as a coadsorbent to reduce dye aggregation. The electrolyte solution, coded A, consisted of 2.0 M 1,3-dimethylimidazolium iodide (DMII), 0.1 M guanidinium thiocyanate (GuNCS), 0.05 M LiI, 0.03 M I_2, and 0.5 M 4-*tert*-butylpyridine (*t*BP) in acetonitrile and

valeronitrile (v/v, 85 : 15). Prior to the measurement, the solar simulator (Sun 3000, ABET Technologies) was calibrated with a certificated *c*-Si solar cell equipped with a KG-3 filter.[58] The device performances were measured using a metallic shadow mask with a square aperture of 4 × 4 mm^2. The obtained photovoltaic parameters are listed in Table 2. It is notable that the recorded cell efficiency of **TF-21** is similar to the previously reported data,[33] while obviously all the newly developed complexes **TF-25**–**TF-28** show improved efficiencies. This appears to be due to the more positive $E^{o\prime}_{ox}$, *i.e.*, a higher oxidation potential *versus* **TF-21**, so that faster dye regeneration is expected, giving a better cell efficiency.[59–61]

The device was further improved by adding tetrabutylammonium deoxycholate [TBA][DOC] to the dye solution, and switching to a different electrolyte system. The addition of the co-adsorbent [TBA][DOC] was expected to conduct the proton-to-TBA exchange at the sensitizer, which in turn could improve the solubility and shift the $E^{o\prime}$* to a more negative value.[62,63] In this approach the alternative electrolyte, now coded as B, consisted of 0.6 M 1,2-dimethyl-3-propylimidazolium iodide (DMPII), 0.1 M LiI, 0.05 M I_2, and 0.5 M 4-*tert*-butylpyridine (*t*BP) in acetonitrile and valeronitrile (v/v, 85 : 15). The higher concentration of LiI in electrolyte B was expected to lower the conduction band edge of the TiO_2 and lead to a faster electron injection and higher J_{SC} for the DSC devices.[64–67]

The resulting photovoltaic parameters are listed in Table 3. To confirm the increase of both the solubility and dye loading by the addition of [TBA][DOC], we re-measured the dye loading under this new condition. As expected, the loading of **TF-21** was notably increased, by 19%, and the reference **TF-21** device now afforded an improved conversion efficiency (η) of 6.44%. In the meantime, DSCs of the respective **TF-25** and **TF-26** under the same conditions also demonstrated a higher loading and much improved efficiencies; namely: η of 7.86 and 7.85%, J_{SC} of 16.92 and 17.12 mA cm^{-2}, V_{OC} of 0.68 and 0.63 V, and a fill factor (FF) of 0.683 and 0.728, as shown in Table 3. The superiority of **TF-25** and **TF-26** over **TF-21** was also attributed to the electron withdrawing property of the extra nitrogen atoms in the ancillary, that shifted the $E^{o\prime}_{ox}$ to the more positive value for a faster dye regeneration (Table 1).[59–61] Moreover, since both **TF-25** and **TF-26** show nearly identical efficiencies, the result implies that the location of the pyrimidinyl substituent imposes an insignificant variation in the device efficiency, due to the retention of both the spatial and electrochemical properties.

Table 3 The performance characteristics of DSCs using electrolyte B and under AM 1.5G illumination

Sensitizers	J_{SC} [mA cm^{-2}]	V_{OC} [V]	FF	η [%]	Dye loading [$\times 10^{-7}$ mol cm^{-2}]
TF-21	15.41	0.64	0.654	6.44	1.69 ± 0.08
TF-25	16.92	0.68	0.683	7.86	2.11 ± 0.05
TF-26	17.12	0.63	0.728	7.85	1.89 ± 0.07
TF-27	17.43	0.62	0.733	7.92	1.04 ± 0.05
TF-28	18.11	0.66	0.729	8.72	1.05 ± 0.04
N749	16.92	0.72	0.727	8.86	

Upon further modification of **TF-26**, by decoration of either the thienyl (**TF-27**) or EDOT (**TF-28**) substituent, the device efficiency increased to 7.92% for **TF-27** and more prominently to 8.72% for **TF-28**. These improvements were attributed to both a better dye loading and light harvesting effect, but the increment was smaller for the thienyl derivative **TF-27** than that of the EDOT functionalized **TF-28**. While the exact cause is unclear, we suspect it could be related to the faster charge recombination,[68] which reduced both the J_{SC} and V_{OC}, as shown by the inferior device performance of **TF-27** (η = 5.32%) *vs.* that of **TF-26** (η = 7.08%) and **TF-28** (η = 6.00%) recorded under a lower dye loading and with electrolyte A (*cf.* Table 2).

The corresponding *J*–*V* characteristics and incident photon-to-current conversion efficiency (IPCE) action spectra are shown in Fig. 4. The IPCE profiles of all the sensitizers (*i.e.* **TF-25**–**TF-28**) clearly reveal a significant improvement over **TF-21** in the region 400–700 nm, and we attributed this to the more positive $E^{o\prime}_{ox}$ and the higher driving force for dye regeneration with the iodide-electrolyte. In Fig. 4(b), the **TF-28** sensitizer, with an EDOT appendage, showed the highest J_{SC} of 18.11 mA cm^{-2}, which is also in agreement with the higher IPCE (by a deviation of <10%) over the solar spectral region. Thus, coupled with the V_{OC} of 0.66 V and FF of 0.729, **TF-28** gave the highest conversion efficiency of 8.72%. On the other hand, the **TF-27** device did not perform with an equivalent efficiency, despite showing a similar spectrum profile and absorptivity *versus* that of **TF-28**.

For an intimate comparison to the pristine sensitizer **N749**, we also fabricated a reference DSC device using identical cell parameters and the electrolyte B (*cf.* Table 3). This reference device showed an essentially identical value for the overall efficiency, but with a slightly lower J_{SC} and higher V_{OC} *versus* our best sensitizer **TF-28** in this study. The variations of the J_{SC} and

Table 2 The performance characteristics of DSCs using electrolyte A and under AM 1.5G illumination

Sensitizers	J_{SC} [mA cm^{-2}]	V_{OC} [V]	FF	η [%]	Dye loading[a] [$\times 10^{-7}$ mol cm^{-2}]
TF-21	10.54	0.58	0.704	4.31	1.42 ± 0.08
TF-25	15.25	0.64	0.709	6.92	1.55 ± 0.08
TF-26	15.34	0.63	0.733	7.08	1.42 ± 0.06
TF-27	12.04	0.59	0.748	5.32	0.88 ± 0.01
TF-28	13.19	0.61	0.746	6.00	0.79 ± 0.01

[a] The value was calculated from the MLCT band ratio for desorbed dye solution *versus* (0.01 mM) reference solution in mixed MeOH and water (v/v, 1 : 1) with 0.1 M of added TBAOH.

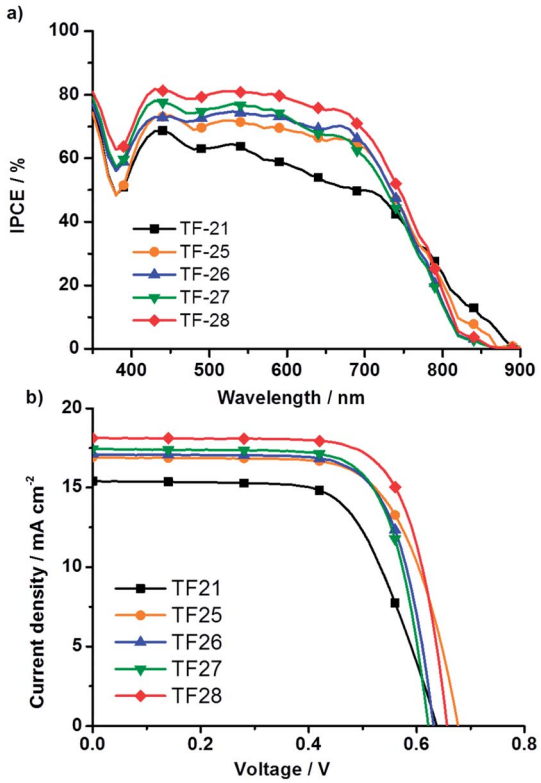

Fig. 4 IPCE action diagram and *J*–*V* characteristics for devices fabricated using the electrolyte B.

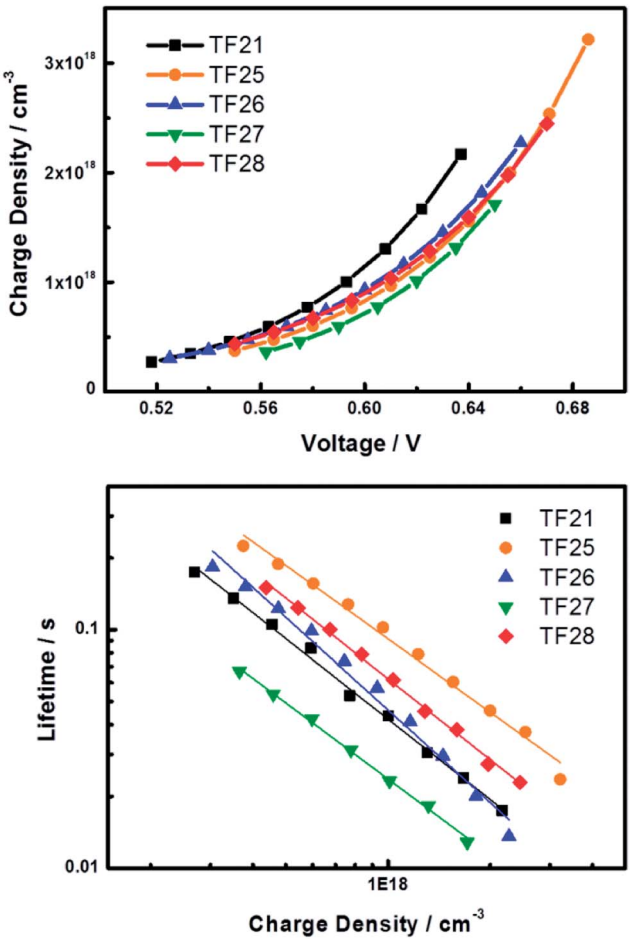

Fig. 5 (a) TiO_2 electron density *versus* voltage deduced from charge extraction measurements and (b) electron lifetime *versus* TiO_2 electron density deduced from transient photovoltage measurements for DSC devices containing **TF-21** and **TF-25**–**TF-28** dyes. The cell voltage was controlled *via* tuning the illumination from a halogen lamp.

V_{OC} between **TF-28** to **N749** could be due to the better light harvesting property and faster charge recombination, a result of the introduction of the EDOT appendage at the ancillary chelate of **TF-28.**

To further probe the device performances, measurements of the charge extraction (CE) and transient photovoltage (TPV) decay were carried out, for which the relevant data are shown in Fig. 5(a) and (b). The differences in the V_{OC} between the cells can generally be explained by shifts in the TiO_2 conduction band edge (manifested by the shift of the exponential distribution of the experimental data measured by CE) and/or by the TiO_2 recombination lifetimes (investigated *via* TPV measurements).[69,70] As can be seen, except for **TF-21** which has a slightly lower V_{OC} at a fixed photo-induced charge density due to a downward shift of the band edge, all the other DSC devices show a very similar V_{OC}, indicating that the conduction band potentials are similar in the cells **TF-25**–**TF-28.** In Fig. 5(b), the transient photovoltage measurements at a fixed charge density indicate that the device made with **TF-25** has the longest electron lifetime, while **TF-27** is the shortest among all the others. The trend of the electron lifetime of these TF sensitizers seems to be in good agreement with the V_{OC} of the devices (Table 2), suggesting that the conduction band edge of TiO_2 is less influential to the observed V_{OC}.

Then, electrochemical impedance spectroscopy was also utilized to analyze the resistance to charge recombination in these devices. Fig. 6 shows the Nyquist plots measured in the dark at a forward bias, the same as the respective V_{OC} tested under a one-sun illumination. The impedance spectra are composed of two semicircles, in which the left (smaller cycle) one depicts the electrochemical reaction at the Pt–electrolyte interface, and the right (larger cycle) one represent the

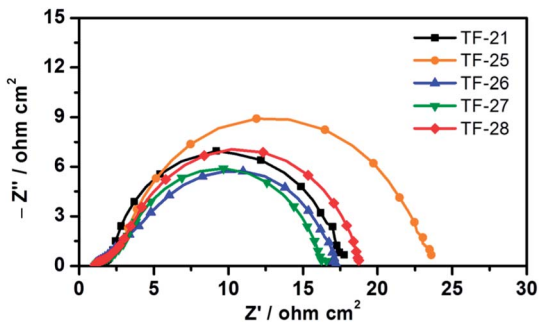

Fig. 6 Electrochemical impedance spectra of DSC devices tested in dark with an external bias as each corresponding V_{OC} under one-sun illumination.

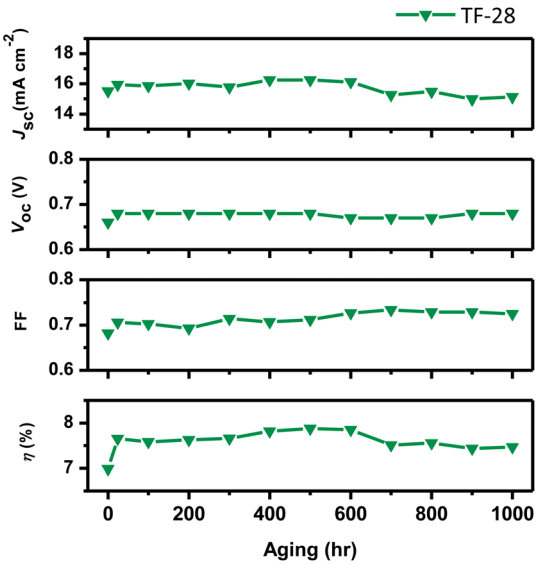

Fig. 7 Device performances of TF-28 under a one-sun light soaking, at 60 °C, for 1000 h.

impedance characteristics of the charge recombination (R_r) at the TiO_2-dye–electrolyte interface.[71–73] The radii of the right series of semicircles indicates R_r to be in the order **TF-25** > **TF-28** > **TF-21** > **TF-26** ≈ **TF-27** and, thus, the dark currents (J_{dark}) appear as an inverse trend, which are consistent with the previous TPV results.

To test the stability of the Ru(II) sensitizers, the highest efficiency device, **TF-28**, was subjected to a light soaking test at 60 °C, for 1000 h, after adopting a low-volatility electrolyte composed of 0.6 M PMII, 0.15 M I_2, 0.1 M GuNCS, and 0.5 M NBB (*N*-butyl-1*H*-benzimidazole) in butyronitrile (BN).[74] With a duration of 1000 h, the J_{SC}, V_{OC}, FF, and η were steady until 600 h and then decreased (Fig. 7). The η_{max} of 7.87% was located around 500 h. The decline of the efficiency, defined as $(\eta_{max} - \eta_{1000h})/\eta_{max}$, was 5.2% which is close to other data reported by our group.[33] This result reconfirmed that the bis-tridentate architecture was stable to the applied thermal stress, under simulated solar irradiation.

Conclusion

In summary, two new types of terdentate ancillary ligands, namely: H_2pzppm (**L5**) and H_2pzpypm (**L6**) and the derivatives (**L6.1** and **L6.2**), were synthesized and employed to construct four bis-tridentate, thiocyanate-free Ru(II) complexes **TF-25**–**TF-28**. The substitution of the pyrimidine for pyridinyl and the phenyl group in the reference **TF-21**, yielded **TF-25** and **TF-26**, respectively, which successfully increased the ground state oxidation potentials to a level of 0.93–0.96 V (*vs.* NHE). With the addition of the thienyl and EDOT decorations on the H_2pzpypm ancillary, the resulting **TF-27** and **TF-28** sensitizers exhibited expected hyperchromic and bathochromic effects, respectively, on their UV-vis absorption spectra. The devices made with **TF-25**–**28** all had superior performance over **TF-21**. **TF-27** showed an improved efficiency, up to 7.92%, while **TF-28** demonstrated the highest efficiency of 8.72%, with an average IPCE of 80% over 400–700 nm and an onset wavelength of 860 nm, confirming their usefulness as a guideline for fine-tuning the functional DSC sensitizers.

Experimental section

General procedures

All the reactions were performed under a nitrogen atmosphere. The solvents were distilled from the appropriate drying agents, prior to use. Commercially available reagents were used, without further purification. All the reactions were monitored by TLC with pre-coated silica gel plates (Merck, 0.20 mm with a fluorescent indicator UV254). The compounds were visualized with UV irradiation at 254 or 365 nm. Flash column chromatography was carried out using silica gel obtained from Merck (230–400 mesh). The mass spectra were obtained on a JEOL SX-102A instrument, operating in the electron impact (EI) or fast atom bombardment (FAB) modes. The ^{1}H and ^{19}F NMR spectra were recorded on a Bruker-400 or INOVA-500 instrument; the chemical shifts are quoted with respect to the internal standard, tetramethylsilane. The elemental analysis was carried out with a Heraeus CHN–O Rapid Elementary Analyzer. The photophysical data were obtained using an Edinburgh fluorescence spectrometer FLS928P. Details of the synthetic protocols for the tri-dentate ancillary chelates and the procedures for the DSC cell fabrication and measurement are all given in the ESI.†

Synthesis of TF-25

A mixture of 4-(3-(trifluoromethyl)-1*H*-pyrazol-5-yl)-2-(3-(trifluoromethyl)phenyl) pyrimidine (114 mg, 0.32 mmol), Ru(tectpy)Cl_3 (204 mg, 0.32 mmol) and KOAc (156 mg, 1.60 mmol) in 30 mL of xylenes was heated at 140 °C, under stirrin,g for 15 h. After the removal of solvent, the crude product of **TF-25**-Et was purified by silica gel column chromatography (ethyl acetate–hexane = 1 : 2). After that, the resulting solid was dissolved in a mixture of acetone (20 mL) and 1 N NaOH solution (1.0 mL). For the hydrolysis, the mixture was stirred at room temperature under nitrogen for 5 h. The solvent was removed, and the residue was dissolved in H_2O (5 mL). This solution was titrated with 2 N $HCl_{(aq)}$ to pH = 3, to afford a brown precipitate. This brown product was washed with acetone and ethyl acetate in sequence, to yield the final product. Yield: 187 mg, 72%. All the other Ru(II) derivatives, *e.g.* **TF-26**–**TF-28**, were synthesized from Ru(tectpy)Cl_3 and the respective ancillary chelates, using identical procedures.

Selected spectral data of TF-25

MS (FAB, ^{102}Ru): *m*/*z* 824 (823) $[M + 1]^+$. ^{1}H NMR (400 MHz, d_6-DMSO,298 K): δ 9.39 (s, 2H), 9.15 (s, 2H), 8.14–8.16 (m, 2H), 7.60–7.63 (m, 4H), 7.47 (s, 1H), 6.76 (d, J_{HH} = 7.6 Hz, 1H), 5.68 (d, J_{HH} = 8 Hz, 1H); ^{19}F NMR (376 MHz, d_6-DMSO, 298 K): δ −58.54 (s, 3F), −60.64 (s, 3F). Anal. calcd for $C_{33}H_{17}F_6N_7O_6Ru \cdot 2H_2O$: C, 46.16; N, 11.42; H, 2.47. Found: C, 46.09; N, 11.31; H, 2.15%.

Selected spectral data of TF-26

MS (FAB, ^{102}Ru): *m*/*z* 825 $(M + 1)^+$. ^{1}H NMR (400 MHz, d_6-DMSO, 298 K): δ 9.31 (s, 2H), 9.11 (s, 2H), 8.33–8.28 (m, 2H), 8.22 (t, J_{HH} = 8 Hz, 1H), 7.64 (dd, J_{HH} = 6 Hz, 2H), 7.59 (d, J_{HH} = 6 Hz, 2H), 7.26 (s, 1H), 7.13 (s, 1H). ^{19}F NMR (376 MHz, d_6-DMSO, 298 K): δ −58.36 (s, 3F), −68.33 (s, 3F). Anal. calcd for $C_{32}H_{16}F_6N_8O_6$-Ru·2H_2O: C, 44.71; N, 13.04; H, 2.35. Found: C, 44.79; N, 12.70; H, 2.46%.

Selected spectral data of TF-27

MS (FAB, ^{102}Ru): *m*/*z* 991 $(M + 1)^+$. ^{1}H NMR (400 MHz, d_6-DMSO, 298 K): δ 9.32 (s, 2H), 9.12 (s, 2H), 8.64 (s, 1H), 8.27 (s, 1H), 8.02 (d, J_{HH} = 3.6 Hz, 1H), 7.70 (d, J_{HH} = 6 Hz, 2H), 7.63 (d, J_{HH} = 6 Hz, 2H), 7.41 (s, 1H), 7.15 (s, 1H), 7.11 (d, J_{HH} = 3.6 Hz, 1H), 2.95 (t, J_{HH} = 8 Hz, 2H), 1.74 (quin, J_{HH} = 8 Hz, 2H), 1.40–1.31 (m, 6H), 0.89 (t, J_{HH} = 8 Hz, 3H). ^{19}F NMR (376 MHz, d_6-DMSO, 298 K): δ −58.38 (s, 3F), −68.22 (s, 3F). Anal. calcd for $C_{42}H_{30}F_6N_8O_6RuS·H_2O$: C, 50.05; N, 11.12; H, 3.20. Found: C, 50.28; N, 11.01; H, 3.10%.

Selected spectral data of TF-28

MS (FAB, ^{102}Ru): *m*/*z* 1049 $(M + 1)^+$. ^{1}H NMR (400 MHz, d_6-DMSO, 298 K): δ 9.31 (s, 2H), 9.12 (s, 2H), 8.49 (s, 1H), 8.39 (s, 1H), 7.68 (d, J_{HH} = 5.6 Hz, 2H), 7.64 (d, J_{HH} = 5.6 Hz, 2H), 7.36 (s, 1H), 7.12 (s, 1H), 4.56–4.51 (m, 2H), 4.41–4.35 (m, 2H), 2.76 (t, J_{HH} = 8 Hz, 2H), 1.67 (quin, J_{HH} = 8 Hz, 2H), 1.45–1.36 (m, 6H), 1.07 (t, J_{HH} = 8 Hz, 3H). ^{19}F NMR (376 MHz, d_6-DMSO, 298 K): δ −58.33 (s, 3F), −68.24 (s, 3F). Anal. calcd for $C_{44}H_{32}F_6N_8O_8$-RuS·2H_2O: C, 48.76; N, 10.34; H, 3.35. Found: C, 48.63; N, 10.02; H, 3.04%.

Acknowledgements

This work was supported by the National Science Council of Taiwan. The computations were conducted at the National Center for High-Performance Computing (NCHC) and we are grateful to the NCHC for their computer time and facilities.

References

1 M. K. Nazeeruddin, A. Kay, I. Rodicio, R. Humphry-Baker, E. Mueller, P. Liska, N. Vlachopoulos and M. Grätzel, *J. Am. Chem. Soc.*, 1993, **115**, 6382.
2 M. Grätzel, *Acc. Chem. Res.*, 2009, **42**, 1788.
3 A. Yella, H.-W. Lee, H. N. Tsao, C. Yi, A. K. Chandiran, M. K. Nazeeruddin, E. W.-G. Diau, C.-Y. Yeh, S. M. Zakeeruddin and M. Grätzel, *Science*, 2011, **334**, 629.
4 M. J. Griffith, K. Sunahara, P. Wagner, K. Wagner, G. G. Wallace, D. L. Officer, A. Furube, R. Katoh, S. Mori and A. J. Mozer, *Chem. Commun.*, 2012, **48**, 4145.
5 B. E. Hardin, H. J. Snaith and M. D. McGehee, *Nat. Photonics*, 2012, **6**, 162.
6 M. K. Nazeeruddin, P. Péchy, T. Renouard, S. M. Zakeeruddin, R. Humphry-Baker, P. Comte, P. Liska, L. Cevey, E. Costa, V. Shklover, L. Spiccia, G. B. Deacon, C. A. Bignozzi and M. Grätzel, *J. Am. Chem. Soc.*, 2001, **123**, 1613.
7 Y. Chiba, A. Islam, R. Komiya, N. Koide and L. Han, *Appl. Phys. Lett.*, 2006, **88**, 223505.
8 H. Ozawa, R. Shimizu and H. Arakawa, *RSC Adv.*, 2012, **2**, 3198.
9 P. Wang, S. M. Zakeeruddin, J. E. Moser, M. K. Nazeeruddin, T. Sekiguchi and M. Grätzel, *Nat. Mater.*, 2003, **2**, 402.
10 M. K. Nazeeruddin, F. De Angelis, S. Fantacci, A. Selloni, G. Viscardi, P. Liska, S. Ito, B. Takeru and M. Grätzel, *J. Am. Chem. Soc.*, 2005, **127**, 16835.
11 T. Bessho, E. Yoneda, J.-H. Yum, M. Guglielmi, I. Tavernelli, H. Imai, U. Rothlisberger, M. K. Nazeeruddin and M. Grätzel, *J. Am. Chem. Soc.*, 2009, **131**, 5930.
12 P. G. Bomben, T. J. Gordon, E. Schott and C. P. Berlinguette, *Angew. Chem., Int. Ed.*, 2011, **50**, 10682.
13 F. Gajardo, M. Barrera, R. Vargas, I. Crivelli and B. Loeb, *Inorg. Chem.*, 2011, **50**, 5910.
14 K. C. D. Robson, B. D. Koivisto, A. Yella, B. Sporinova, M. K. Nazeeruddin, T. Baumgartner, M. Grätzel and C. P. Berlinguette, *Inorg. Chem.*, 2011, **50**, 5494.
15 Y. Qin and Q. Peng, *Int. J. Photoenergy*, 2012, **2012**, 291579.
16 S. P. Singh, K. S. V. Gupta, G. D. Sharma, A. Islam and L. Han, *Dalton Trans.*, 2012, **41**, 7604.
17 K. C. D. Robson, P. G. Bomben and C. P. Berlinguette, *Dalton Trans.*, 2012, **41**, 7814.
18 T. Funaki, H. Funakoshi, N. Onozawa-Komatsuzaki, K. Kasuga, K. Sayama and H. Sugihara, *Chem. Lett.*, 2012, **41**, 647.
19 L. E. Polander, A. Yella, B. F. E. Curchod, A. N. Ashari, J. Teuscher, R. Scopelliti, P. Gao, S. Mathew, J.-E. Moser, I. Tavernelli, U. Rothlisberger, M. Gratzel, M. K. Nazeeruddin and J. Frey, *Angew. Chem., Int. Ed.*, 2013, **52**, 8731.
20 T. Funaki, N. Onozawa-Komatsuzaki, K. Kasuga, K. Sayama and H. Sugihara, *Inorg. Chem. Commun.*, 2013, **35**, 281.
21 C. Dragonetti, A. Colombo, M. Magni, P. Mussini, F. Nisic, D. Roberto, R. Ugo, A. Valore, A. Valsecchi, P. Salvatori, M. G. Lobello and F. D. Angelis, *Inorg. Chem.*, 2013, **52**, 10723.
22 G. D. Sharma, S. P. Singh, R. Kurchania and R. J. Ball, *RSC Adv.*, 2013, **3**, 6036.
23 P. T. Nguyen, A. R. Andersen, E. M. Skou and T. Lund, *Sol. Energy Mater. Sol. Cells*, 2010, **94**, 1582.
24 S. H. Wadman, J. M. Kroon, K. Bakker, M. Lutz, A. L. Spek, G. P. M. van Klink and G. van Koten, *Chem. Commun.*, 2007, 1907.
25 S. H. Wadman, M. Lutz, D. M. Tooke, A. L. Spek, F. Hartl, R. W. A. Havenith, G. P. M. van Klink and G. van Koten, *Inorg. Chem.*, 2009, **48**, 1887.
26 K. C. D. Robson, B. D. Koivisto and C. P. Berlinguette, *Inorg. Chem.*, 2012, **51**, 1501.
27 B. Schulze, D. G. Brown, K. C. D. Robson, C. Friebe , M. Jäger , E. Birckner, C. P. Berlinguette and U. S. Schubert , *Chem.–Eur. J.*, 2013, **19**, 14171.
28 M. Chandrasekharam, T. Suresh, S. P. Singh, B. Priyanka, K. Bhanuprakash, A. Islam, L. Han and M. Lakshmi Kantam, *Dalton Trans.*, 2012, **41**, 8770.

29 S.-W. Wang, K.-L. Wu, E. Ghadiri, M. G. Lobello, S.-T. Ho, Y. Chi, J.-E. Moser, F. De Angelis, M. Grätzel and M. K. Nazeeruddin, *Chem. Sci.*, 2013, **4**, 2423.
30 T. Moehl, H. N. Tsao, K.-L. Wu, H.-C. Hsu, Y. Chi, E. Ronca, F. De Angelis, M. K. Nazeeruddin and M. Grätzel, *Chem. Mater.*, 2013, **25**, 4497.
31 K.-L. Wu, H.-C. Hsu, K. Chen, Y. Chi, M.-W. Chung, W.-H. Liu and P.-T. Chou, *Chem. Commun.*, 2010, **46**, 5124.
32 C.-C. Chou, K.-L. Wu, Y. Chi, W.-P. Hu, S. J. Yu, G.-H. Lee, C.-L. Lin and P.-T. Chou, *Angew. Chem., Int. Ed.*, 2011, **50**, 2054.
33 C.-W. Hsu, S.-T. Ho, K.-L. Wu, Y. Chi, S.-H. Liu and P.-T. Chou, *Energy Environ. Sci.*, 2012, **5**, 7549.
34 K.-L. Wu, W.-P. Ku, J. N. Clifford, E. Palomares, S.-T. Ho, Y. Chi, S.-H. Liu, P.-T. Chou, M. K. Nazeeruddin and M. Grätzel, *Energy Environ. Sci.*, 2013, **6**, 859.
35 K.-L. Wu, W.-P. Ku, S.-W. Wang, A. Yella, Y. Chi, S.-H. Liu, P.-T. Chou, M. K. Nazeeruddin and M. Grätzel, *Adv. Funct. Mater.*, 2013, **23**, 2285.
36 M. A. Elban, W. Sun, B. M. Eisenhauer, R. Gao and S. M. Hecht, *Org. Lett.*, 2006, **8**, 3513.
37 X. Zheng, B. Song and B. Xu, *Eur. J. Org. Chem.*, 2010, **2010**, 4376.
38 S. C. Ceide and A. G. Montalban, *Tetrahedron Lett.*, 2006, **47**, 4415.
39 A. Miyashita, Y. Suzuki, K. Ohta and T. Higashino, *Heterocycles*, 1994, **39**, 345.
40 J. Easmon, G. Puerstinger, K.-S. Thies, G. Heinisch and J. Hofmann, *J. Med. Chem.*, 2006, **49**, 6343.
41 M.-W. Chung, T.-Y. Lin, C.-C. Hsieh, K.-C. Tang, H. Fu, P.-T. Chou, S.-H. Yang and Y. Chi, *J. Phys. Chem. A*, 2010, **114**, 7886.
42 J. Suh and W. J. Kwon, *Bioorg. Chem.*, 1998, **26**, 103.
43 H. Ait-Haddou, E. Bejan, J.-C. Daran, G. G. A. Balavoine, F. Berruyer-Penaud, L. Bonazzola, H. Smaoui-Chaabouni and E. Amouyal, *J. Chem. Soc., Dalton Trans.*, 1999, 3095.
44 K.-S. Chen, W.-H. Liu, Y.-H. Wang, C.-H. Lai, P.-T. Chou, G.-H. Lee, K. Chen, H.-Y. Chen, Y. Chi and F.-C. Tung, *Adv. Funct. Mater.*, 2007, **17**, 2964.
45 A. Hagfeldt, G. Boschloo, L. Sun, L. Kloo and H. Pettersson, *Chem. Rev.*, 2010, **110**, 6595.
46 Y.-S. Yen, Y.-C. Chen, Y.-C. Hsu, H.-H. Chou, J. T. Lin and D.-J. Yin, *Chem.–Eur. J.*, 2011, **17**, 6781.
47 J.-F. Yin, M. Velayudham, D. Bhattacharya, H.-C. Lin and K.-L. Lu, *Coord. Chem. Rev.*, 2012, **256**, 3008.
48 Y.-S. Yen, H.-H. Chou, Y.-C. Chen, C.-Y. Hsu and J. T. Lin, *J. Mater. Chem.*, 2012, **22**, 8734.
49 Y. Ooyama and Y. Harima, *ChemPhysChem*, 2012, **13**, 4032.
50 S.-R. Li, C.-P. Lee, H.-T. Kuo, K.-C. Ho and S.-S. Sun, *Chem.–Eur. J.*, 2012, **18**, 12085.
51 B.-G. Kim, K. Chung and J. Kim, *Chem.–Eur. J.*, 2013, **19**, 5220.
52 Y. Wu and W. Zhu, *Chem. Soc. Rev.*, 2013, **42**, 2039.
53 F. Gao, Y. Wang, D. Shi, J. Zhang, M. Wang, X. Jing, R. Humphry-Baker, P. Wang, S. M. Zakeeruddin and M. Grätzel, *J. Am. Chem. Soc.*, 2008, **130**, 10720.
54 W.-H. Liu, I.-C. Wu, C.-H. Lai, C.-H. Lai, P.-T. Chou, Y.-T. Li, C.-L. Chen, Y.-Y. Hsu and Y. Chi, *Chem. Commun.*, 2008, 5152.
55 K. Lim, C. Kim, J. Song, T. Yu, W. Lim, K. Song, P. Wang, N. Zu and J. Ko, *J. Phys. Chem. C*, 2011, **115**, 22640.
56 W. Zeng, Y. Cao, Y. Bai, Y. Wang, Y. Shi, M. Zhang, F. Wang, C. Pan and P. Wang, *Chem. Mater.*, 2010, **22**, 1915.
57 A. Listorti, B. O'Regan and J. R. Durrant, *Chem. Mater.*, 2011, **23**, 3381.
58 X. Yang, M. Yanagida and L. Han, *Energy Environ. Sci.*, 2013, **6**, 54.
59 T. Funaki, H. Funakoshi, O. Kitao, N. Onozawa-Komatsuzaki, K. Kasuga, K. Sayama and H. Sugihara, *Angew. Chem., Int. Ed.*, 2012, **51**, 7528.
60 F.-C. Hu, S.-W. Wang, M. Planells, N. Robertson, H. Padhy, B.-S. Du, Y. Chi, P.-F. Yang, H.-W. Lin, G.-H. Lee and P.-T. Chou, *ChemSusChem*, 2013, **6**, 1366.
61 H.-H. Yeh, S.-T. Ho, Y. Chi, J. N. Clifford, E. Palomares, S.-H. Liu and P.-T. Chou, *J. Mater. Chem. A*, 2013, **1**, 7681.
62 K.-L. Wu, S.-T. Ho, C.-C. Chou, Y.-C. Chang, H.-A. Pan, Y. Chi and P.-T. Chou, *Angew. Chem., Int. Ed.*, 2012, **51**, 5642.
63 C.-C. Chou, F.-C. Hu, H.-H. Yeh, H.-P. Wu, Y. Chi, J. N. Clifford, E. Palomares, S.-H. Liu, P.-T. Chou and G.-H. Lee, *Angew. Chem., Int. Ed.*, 2014, **53**, 178.
64 A. C. Onicha and F. N. Castellano, *J. Phys. Chem. C*, 2010, **114**, 6831.
65 Q. Yu, Y. Wang, Z. Yi, N. Zu, J. Zhang, M. Zhang and P. Wang, *ACS Nano*, 2010, **4**, 6032.
66 P. G. Johansson, J. G. Rowley, A. Taheri, G. J. Meyer, S. P. Singh, A. Islam and L. Han, *Langmuir*, 2011, **27**, 14522.
67 Y. Shi, Y. Wang, M. Zhang and X. Dong, *Phys. Chem. Chem. Phys.*, 2011, **13**, 14590.
68 K. C. D. Robson, K. Hu, G. J. Meyer and C. P. Berlinguette, *J. Am. Chem. Soc.*, 2013, **135**, 1961.
69 D. Credgington and J. R. Durrant, *J. Phys. Chem. Lett.*, 2012, **3**, 1465.
70 P. R. F. Barnes, K. Miettunen, X. Li, A. Y. Anderson, T. Bessho, M. Grätzel and B. C. O'Regan, *Adv. Mater.*, 2013, **25**, 1881.
71 S. M. Zakeeruddin and M. Grätzel, *Adv. Funct. Mater.*, 2009, **19**, 2187.
72 J. Halme, P. Vahermaa, K. Miettunen and P. Lund, *Adv. Mater.*, 2010, **22**, E210.
73 F. Fabregat-Santiago, J. Bisquert, G. Garcia-Belmonte, G. Boschloo and A. Hagfeldt, *Sol. Energy Mater. Sol. Cells*, 2005, **87**, 117.
74 F. Sauvage, S. Chhor, A. Marchioro, J.-E. Moser and M. Grätzel, *J. Am. Chem. Soc.*, 2011, **133**, 13103.

